Structural response of bijels stabilized by ellipsoidal magnetic particles

Nikhil Karthikeyan[1][0000−0003−3746−2367] and
Ulf D. Schiller[1,2][0000−0001−8941−1284]

[1] Department of Materials Science and Engineering, 201 DuPont Hall, University of Delaware, Newark, DE 19716, USA
[2] Department of Computer and Information Sciences, 18 Amstel Ave, University of Delaware, Newark, DE 19716, USA
{nkarthi,uschill}@udel.edu

Abstract. Bicontinuous interfacially jammed emulsion gels (bijels) are soft materials characterized by an interconnected network of fluid domains stabilized by colloidal particles. Their tunable microstructures make them promising candidates for applications in material templating, membrane separations, and drug delivery. In this study, we explore how magnetic fields influence the post-formation structural evolution of bijels stabilized by magnetically responsive ellipsoidal particles. Using hybrid Lattice Boltzmann–Molecular Dynamics simulations, we examine the response of systems stabilized by oblate and prolate particles across a range of magnetic field strengths ($\bar{B} = 0, 0.2, 0.5, 1$). We quantify structural evolution through metrics including domain size, average interfacial tilt angle and six-fold Steinhardt bond orientational order. Our findings reveal that particle shape mediates the extent of anisotropy and domain coarsening, with prolate particles promoting ordering and alignment, while oblate particles tend to disrupt local structure. Finally, we compare bijels formed under an applied field to those exposed post-formation, showing that magnetic alignment can effectively tune microstructure in both cases to an approximately equal degree, highlighting a viable route for post-processing control of responsive bijel materials.

Keywords: particle-stabilized emlsions · lattice Boltzmann methods · emulsion templating.

1 Introduction

Stimuli-responsive emulsions have gained interest for applications in enhanced oil recovery, porous material templates, in-situ reaction separation, and drug delivery scaffolds [36, 2]. These applications rely on microstructure modifications driven by external stimuli, altering the permeability, surface area, and morphology of the emulsion. With advances in particle synthesis and concerns over surfactant toxicity, particle-stabilized emulsions have regained popularity since their discovery by Ramsden and Pickering in 1907 [29, 46]. Stimuli response in

ICCS Camera Ready Version 2025
To cite this paper please use the final published version:
DOI: 10.1007/978-3-031-97564-6_19

these systems has been achieved using pH, temperature, or chemical composition changes [22, 21, 27, 44].

Bicontinuous interfacially jammed emulsion gels (bijels) are of particular interest due to their tortuous, co-continuous domain morphology, making them suitable for membranes, catalyst supports, battery electrodes, and pharmaceutical products [42, 30, 5, 11, 31]. Bijels form through the arrest of spinodal decomposition in partially miscible fluids [35, 14, 37]. During phase separation, the interface sweeps through the system and adsorbs the particles. When the interfacial area matches the cross-sectional area of the particles, the particles jam and arrest the phase separation [35, 14, 37]. Since their discovery in simulations and subsequent experimental synthesis, extensive research has explored various fluid systems for bijel formation, scalable fabrication methods, and potential applications.

Bijels stabilized by ellipsoidal particles exhibit multiple timescales compared to those stabilized by spherical particles [13]. After jamming, capillary interactions drive further reorientation, leading to domain coarsening over longer timescales [13]. Magnetic fields offer a promising external stimulus due to their targeted interactions, biological compatibility, and diverse material applications. The structural response of magnetically responsive materials depends on initial particle orientation, as seen in hydroxyapatite crystals [25]. In Pickering emulsions stabilized by magnetic microspheres, magnetophoresis drives particle movement along field lines [38]. Additionally, particle migration and tilting at interfaces can cause structural deformation and de-emulsification [43, 24]. Given their locally jammed nature, combining anisotropic particle-stabilized bijels with magnetic field control could enable precise microstructural tuning, and has been exhibited to do so during the formation stage of bijels [17].

In this work, we use hybrid Lattice Boltzmann–Molecular Dynamics simulations to investigate the structural evolution of bijels stabilized by magnetically responsive ellipsoidal particles under externally applied magnetic fields. We examine how particle shape and field strength influence domain coarsening, anisotropy, and local particle ordering. Our results show that magnetic fields can induce anisotropy and particle ordering to the applied direction. The shape of the particle affects how the interfacial packing is affected, with prolate particles having increased ordering while oblate particles exhibit lower local ordering due to out-of-plane tilting. Additionally, we compare the effects of applying the magnetic field during versus after bijel formation and find that similar microstructural changes can be achieved in both cases. These findings highlight the potential of magnetic field-driven control as a versatile strategy for post-processing and tuning the structure of active soft materials.

2 Model parameters and simulation setup

Bijels are inherently non-equilibrium materials, formed via the arrest of spinodal decomposition in a binary fluid mixture by interfacially adsorbed particles. This kinetic arrest leads to a bicontinuous structure that is stabilized by particle

ICCS Camera Ready Version 2025
To cite this paper please use the final published version:
DOI: 10.1007/978-3-031-97564-6_19

jamming at the fluid interface. The incompressible Navier–Stokes and advective Cahn–Hilliard equations have been used to model hydrodynamics and phase separation respectively facilitating simulations of bijel systems. Particle adsorption and interfacial jamming are achieved through particle-fluid coupling and interparticle interactions, which prevent further coarsening once the interface area matches the available particle surface area. This setup enables us to simulate the dynamics of a bijel during formation from an initially homogeneous fluid mixture as well as post formation, investigating the effect of particle dynamics on the microstructure of the system. To study magnetically responsive bijels, we additionally include magnetic dipole-dipole interactions and coupling to an external field.

To simulate hydrodynamics and non-ideal liquid mixing, we utilize a D3Q19 lattice Boltzmann method (LBM) that implements the Shan-Chen multicomponent model. It evolves a particle density distribution for species k $f_i^k(\boldsymbol{x},t)$ at time t at grid point $\boldsymbol{x}$ in lattice direction i using a single relaxation time τ or BGK collision operator [26, 4]

$$f_i^k(\boldsymbol{x}+\boldsymbol{c}_i\Delta t, t+\Delta t) = f_i^k(\boldsymbol{x},t) - \frac{\Delta t}{\tau_k}\left[f_i^k(\boldsymbol{x},t) - f_i^{k,\mathrm{eq}}(\rho_k, \boldsymbol{u}_k^{\mathrm{eq}})\right], \tag{1}$$

where $f_i^{k,\mathrm{eq}}(\rho_k, \boldsymbol{u}_k^{\mathrm{eq}})$ denotes an equilibrium distribution that depends on the local fluid density $\rho_k = \sum_k f_i^k$ and velocity $\boldsymbol{u}_k^{\mathrm{eq}}$. The equilibrium distribution $f_i^{k,\mathrm{eq}} = f_i^{\mathrm{eq}}$ is written as a hermitian polynomial expansion of the Maxwell-Boltzmann distribution. When performing a Chapman-Enskog expansion of f, the incompressible Navier-Stokes equation is recovered. Non-ideal mixing in the Shan-Chen multicomponent model is modeled through a non-local interaction force between the fluid components [32, 33]

$$\boldsymbol{F}_k(\boldsymbol{x})\Delta t = -\sum_{k'}\sum_i \frac{w_i}{c_s^2} g_{kk'}\psi_k(\boldsymbol{x})\psi_{k'}(\boldsymbol{x}+\boldsymbol{c}_i)\boldsymbol{c}_i, \tag{2}$$

where $\psi_k(\boldsymbol{x}) = \psi(\rho_k(\boldsymbol{x}))$ represents the effective density of the fluid component k, and $g_{kk'}$ controls the strength of the force between fluids. The force is added to the velocity of the fluids $\boldsymbol{u}_k^{\mathrm{eq}} = \boldsymbol{u}' + \frac{\tau_k}{\rho_k}\boldsymbol{F}_k$, where $\boldsymbol{u}'$ is defined as $\sum_k \frac{\rho_k}{\tau_k}\boldsymbol{u}' = \sum_k \frac{1}{\tau_k}\sum_i f_i^k \boldsymbol{c}_i$. The advective Cahn-Hilliard equation is obtained when performing a Chapman-Enskog expansion of the order parameter, defined as $\phi = \rho_k - \rho_{k'}$. We then couple particles to the fluid based on the approach of Ladd and Aidun, where particles are modeled as rigid bodies that exchange momentum with the fluid and interact through Hertzian contact and lubrication forces with other particles [19, 1, 16]. More information about the specific expressions used to account for particle anisotropy can be found in [7, 40, 17]. We incorporate magnetic interactions using a dipole interparticle potential. Field-particle interactions are handled through coupling to the field B

$$\begin{aligned} \boldsymbol{F} &= (\boldsymbol{m}\cdot\nabla)\,\boldsymbol{B}, \\ \boldsymbol{T} &= \boldsymbol{m}\times\boldsymbol{B}. \end{aligned} \tag{3}$$

ICCS Camera Ready Version 2025
To cite this paper please use the final published version:
DOI: 10.1007/978-3-031-97564-6_19

This model is implemented in LB3D, with further details of the implementation and specific equations given in previous work [16, 13, 6, 41, 17].

The initial configuration is setup using bijels simulated with various magnetic field strengths in a cubic box with side length $n_x = 256\Delta x$. The fluids have volume fraction $\phi_f = 0.5$, fluid density $\rho_f = 0.7\frac{\Delta m}{(\Delta x)^3}$ and kinematic viscosity $\nu_f = c_s^2(\tau - \Delta t/2) = \frac{1}{6}\frac{(\Delta x)^2}{\Delta t}$ at a relaxation rate $\tau = 1\Delta t$. The fluids have a surface tension controlled using the parameter $g_{kk'} = 0.08\frac{(\Delta x)^5}{(\Delta t)^2\Delta m}$. The surface tension at the specified $g_{kk'}$ under these settings is $\sigma = 0.0267\frac{\Delta m}{(\Delta t)^2}$, found using the Young-Laplace law when plotting the fit of the pressure difference between the interior and exterior of a droplet and the radius of the droplet.

The bijels are stabilized with particle volume fraction $\phi_p = 0.1$, corresponding to 812 particles in the system with particle density $\rho_p = 1\frac{\Delta m}{(\Delta x)^3}$. We studied ellipsoidal particles with radii $R_p = 5\Delta x, R_o = 10\Delta x$ for oblate particles $\alpha = \frac{R_p}{R_o} = 0.5$ and $R_p = 12.6\Delta x, R_o = 6.3\Delta x$ for prolate particles $\alpha = 2$. The strength of the Hertzian potential is controlled using $K_H = 100\frac{\Delta m}{(\Delta t)^2\sqrt{\Delta x}}$ and used in line with past works investigating bijels with LB3D. The cutoff distance for the lubrication force was set using $\Delta_c = 2/3\Delta x$ and selected based on recommendation from Ladd et al. and is dependent upon the relaxation time used [19]. A dimensionless applied magnetic field is defined as $\bar{B} = \frac{mB}{\sigma A_{rm}}$ where m is the dipole moment of the particle, B is the numerical value of the applied field and A_{rm} is the surface area of the particle at equilibrium. Its value is variable and defined in each subsection below.

An experimental system will be briefly mentioned to compare the simulation parameters here to a real system. Water-lutidine bijels have been used before when synthesizing bijel templates. A water-lutidine system has a Lower Critical Solution Temperature(LCST) of 37°C. To initiate phase separation of this mixture, the temperature is raised to 40°C. At this temperature, the surface tension between fluids is $2.2 \cdot 10^{-4}$ N/m and the dynamic viscosity of the lutidine rich phase is $2.38 \cdot 10^{-3}$ Pas [12]. Ellipsoidal magnetic articles with equivalent diameter 4 μm and magnetic moment $m \approx 3 \cdot 10^{-14}$ Am^2 can be synthesized through mechanical stretching of polystyrene microparticles and subsequent coating with nickel using physical vapor deposition [9, 10]. This results in a system with $\Delta x = 252$ nm and $\Delta t = 624$ ns resulting in a box length of ≈ 65 μm and a simulation duration of $t = 62.4$ ms.

3 Results

We investigate how the microstructure of bijels stabilized by ellipsoidal particles at a volume fraction $\phi_p = 0.1$ evolves under varying magnetic field strengths $\bar{B} = 0, 0.2, 0.5, 1$.

Figure 1 shows snapshots of the bijel microstructure at the initial and final time steps of the simulation with and without an applied field for bijels stabilized by prolate particles. It illustrates how the particles align with the direction of

ICCS Camera Ready Version 2025
To cite this paper please use the final published version:
DOI: 10.1007/978-3-031-97564-6_19

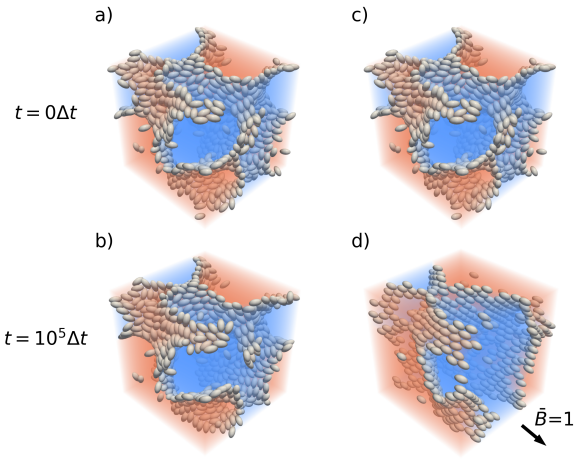

Fig. 1. Evolution of the bijel microstructure stabilized by prolate particles, shown at the initial time step ($t = 0\Delta t$, top row) and after $10^5\Delta t$ (bottom row). The left column (a-b) shows the system with no applied field, while the right column (c-d) shows the effect of an external field of strength $\bar{B} = 1$, indicated by the arrow in panel (d). Upon field application, particles tend to align with the field direction, and the fluid domains deform in response, adopting a distinct anisotropic morphology.

the magnetic field. While reorienting, the particles adopt new interfacial arrangements, resulting in coarsened fluid domains. The effect of domain coarsening can be measured using the average domain size from the first moment of the structure factor, calculated via the Fourier transform of order parameter fluctuations [18]. Our methodology to calculate the domain size is explained in a past publication [17]. We plot the domain size results in Figure 2.

Figure 2 presents the time evolution of the normalized average domain size, where the characteristic length scale is defined using the volume-equivalent spherical particle radius $R = 7.9$. When a magnetic field is applied to a bijel formed in the absence of one, the final average domain size increases by up to 5.2% for bijels stabilized by oblate particles and 2.5% for those stabilized by prolate particles. The coarsening dynamics following field application appear to be similar if the particle shape is the same, as indicated by the comparable slopes of domain size evolution during the intermediate-time regime. Domain coarsening is observed even in the absence of a magnetic field, likely driven by interparticle forces that promote reorientation at the interface, thereby altering the particle monolayer coverage as previously reported by Günther et al. [13].

3.1 Comparisons of stimuli response pre and post jamming

Our earlier work investigated the impact of applying magnetic fields during bijel formation with ellipsoidal particles, revealing microstructural anisotropy and di-

ICCS Camera Ready Version 2025
To cite this paper please use the final published version:
DOI: 10.1007/978-3-031-97564-6_19

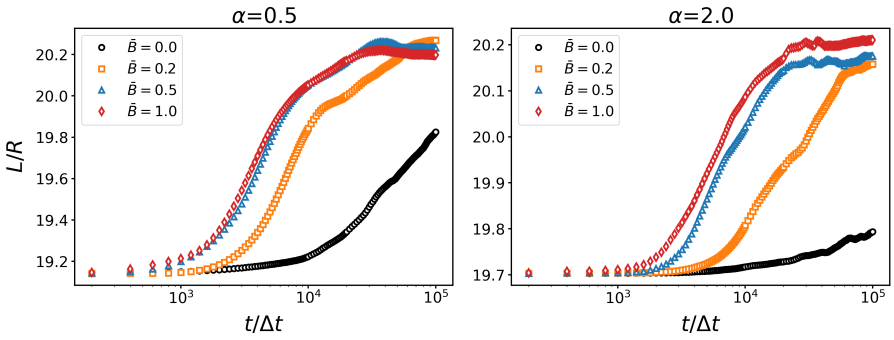

Fig. 2. Time evolution of the characteristic domain size L/R for bijels stabilized by ellipsoidal particles with aspect ratios $\alpha = 0.5$ (left) and $\alpha = 2.0$ (right), under varying field strengths $\bar{B}$. The application of a field causes coarsening to initiate earlier compared to the no-field case. However, once coarsening begins, the domain growth follows a consistent power-law scaling for all nonzero field strengths, distinct from the coarsening observed when no field is applied.

rectional tortuosity, with implications for applications such as battery electrodes, tissue engineering scaffolds, and architected porous media [45, 8, 15, 17]. Here, we investigate whether the degree of domain size change is equivalent when the field is applied during versus after bijel formation. To this end, we compute the difference between domain sizes obtained under these two conditions using the same field strengths, particle shapes, and volume fractions. The results, shown in Figure 3, include both spherically averaged and directional domain sizes and highlight how the timing of field application influences the final microstructure.

For oblate particles ($\alpha = 0.5$), the difference in average domain size, ΔL_1, is non-zero at low field strengths but decreases as $\bar{B}$ increases. This trend suggests that low magnetic fields allow greater flexibility for particle monolayer rearrangement, enabling the domain coarsening observed upon field application. However, the overall differences in domain size remain small, indicating that applying a magnetic field after formation leads to minimal structural changes for bijels stabilized by oblate particles. In contrast, bijels stabilized by prolate particles ($\alpha = 2.0$) exhibit a more pronounced increase in ΔL_1 with increasing field strength, implying that higher fields facilitate further coarsening even after the bijel has formed. Nevertheless, the magnitude of these changes remains within the width of the fluid-fluid interface resolved in the simulation, suggesting that they may not lead to significant differences in macroscopic physical properties. When examining the directional domain sizes, bijels stabilized by oblate particles ($\alpha = 0.5$) show slightly larger domains in both directions at low field strengths. At higher field strengths, however, $\Delta L_{\parallel}$ exceeds that observed when the field is applied during formation, indicating subtle differences in field-induced structural evolution depending on the timing of application. A similar trend is observed

ICCS Camera Ready Version 2025
To cite this paper please use the final published version:
DOI: 10.1007/978-3-031-97564-6_19

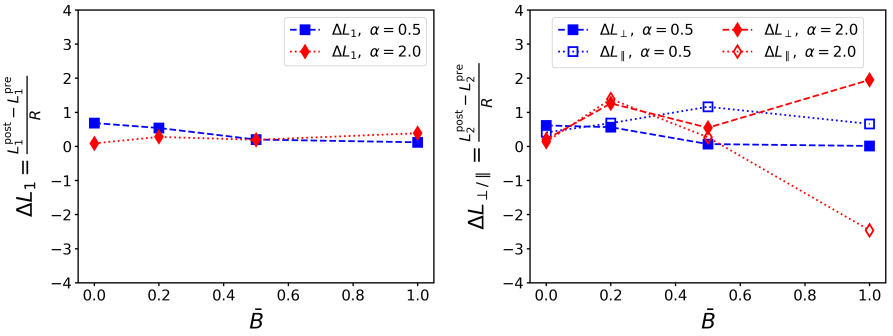

Fig. 3. Differences between the particle radius normalized spherically averaged domain size (left) and directional domain size (right) of bijels stabilized with ellipsoidal particles. The difference in length scales is calculated from the difference between the length scale metric calculated for bijels with a field applied post formation to bijels with the same field applied during formation.

for bijels stabilized by prolate particles ($\alpha = 2.0$) at $\bar{B} = 1$, where a substantial anisotropy develops, with $\Delta L_\parallel$ significantly exceeding $\Delta L_\perp$. This is thought to arise from sensitivity of the response to the initial configuration of particles.

3.2 Effect of the particle monolayer

The magnetic field exerts a torque onto the particles, rotating them towards the magnetic field. Previous investigations have shown that the orientational ordering of the particles increase over time upon application of a magnetic field in bijels stabilized by magnetically responsive ellipsoidal particles [17]. Here, we focus on how the reorientation affects how the particles arrange at the interface, as seen in Figure 4. Initially, monolayer particles are randomly oriented and lie flat on the interface. Upon applying a magnetic field, they align with the field direction, causing structural changes from particle unjamming and re-jamming.

Due to the irreversible adsorption of microparticles at fluid interfaces, structural evolution in bijels primarily arises from particle monolayer unjamming and re-jamming events, or through deformation of the interface. Particles tend to adsorb with their largest cross-sectional area aligned to the interface. Despite being strongly adsorbed, particles retain the ability to reorient in response to external stimuli, such as an applied magnetic field. Prior work by Davies et al. demonstrated that a minimum field strength of $\bar{B} = 0.2$ is required to induce out-of-plane tilting for particles with geometries similar to those used in this study [7]. To investigate the dynamics of monolayer rearrangement upon field application, we analyze the orientation of particles through the average interfacial angle, ψ. The method for computing ψ is detailed in Karthikeyan and Schiller [17]. ψ is calculated for each interfacially adsorbed particle and averaged to obtain $\langle\psi\rangle$. The time evolution of $\langle\psi\rangle$ is presented in Figure 5.

ICCS Camera Ready Version 2025
To cite this paper please use the final published version:
DOI: 10.1007/978-3-031-97564-6_19

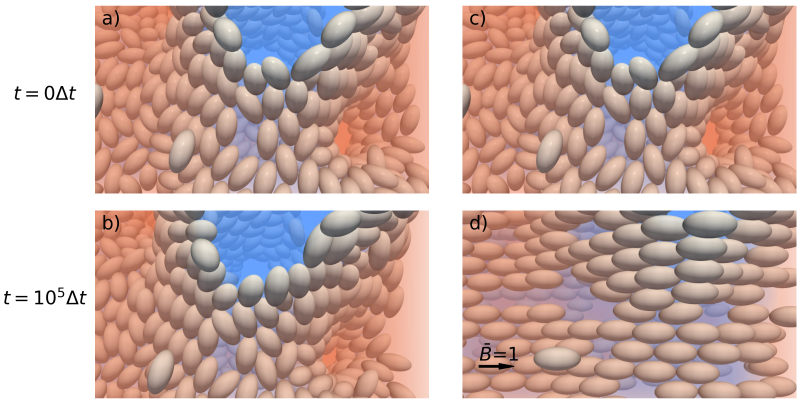

Fig. 4. Evolution of the a prolate particle monolayer shown at the initial timestep ($t = 0\Delta t$, top row) and after $10^5\Delta t$ (bottom row). The left column (a-b) shows the system with no applied field, while the right column (c-d) shows the effect of an external field of strength $\bar{B} = 1$, indicated by the arrow in panel (d). Upon field application, particles tend to align with the field direction causing differences in how the particles arrange at the interface.

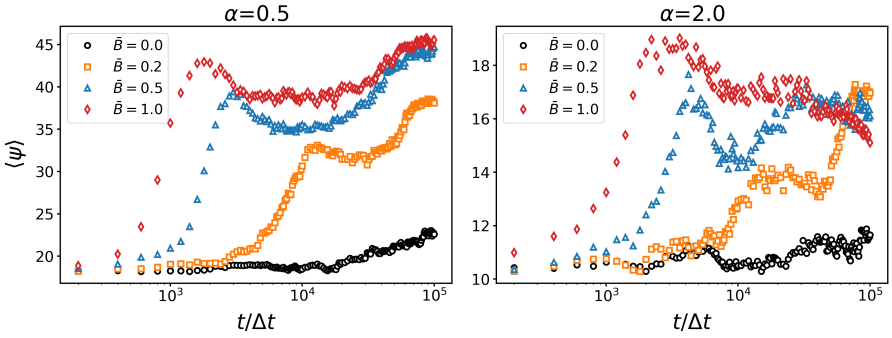

Fig. 5. Time evolution of the average interfacial tilt angle $\langle\psi\rangle$ for bijels stabilized by oblate particles ($\alpha = 0.5$, left) and prolate particles ($\alpha = 2.0$, right) under varying magnetic field strengths $\bar{B}$.

ICCS Camera Ready Version 2025
To cite this paper please use the final published version:
DOI: 10.1007/978-3-031-97564-6_19

Figure 5 shows the evolution of the average tilt angle $\langle\psi\rangle$ for ellipsoid-stabilized bijels under an applied magnetic field. Initially, $\langle\psi\rangle$ increases as particles begin to tilt in response to the field, followed by a brief decrease, and then a gradual increase or decrease depending on the particle shape. This suggests that particles initially lie nearly flat on the interface but tilt under the influence of the magnetic field. As the system evolves, $\langle\psi\rangle$ reaches a plateau, corresponding to a regime where capillary forces reorient the fluid interface to accommodate the new particle alignment. Once the interface settles into this reoriented configuration, the particle monolayer becomes jammed again, leading to the observed plateau in $\langle\psi\rangle$ at intermediate to late times.

The initial tilting rate, duration of the plateau, and final tilt angle all increase with field strength, underscoring the competition between magnetic torques driving particle reorientation and interfacial capillary forces resisting deformation. As the particles align with the magnetic field, the interface deforms to minimize interfacial free energy, ultimately contributing to the anisotropic domain structures characterized for magnetically responsive bijels. Differences in this behavior emerge between oblate and prolate particles. Bijels stabilized by oblate particles exhibit a more pronounced increase in $\langle\psi\rangle$ after field application, owing to their tendency to stack vertically when aligned with the field. In contrast, prolate particles preferentially adopt side-to-side or end-to-end configurations, which favors flatter orientations at the interface. This difference results in divergent late-time behaviors. For oblate particles, $\langle\psi\rangle$ continues to increase as particles gradually tilt out of the interface, while for prolate particles, $\langle\psi\rangle$ decreases as particles reorient to optimize packing by lying flatter on the interface.

To quantitatively assess the local arrangement of particles at the interface, we compute the ensemble-averaged Steinhardt bond orientational order parameter Q_6 [34, 20, 23]. These parameters characterize the local structural ordering by projecting the orientations of neighboring particles onto spherical harmonics Y_{lm} of degree l, and are defined as

$$Q_l(i) = \sqrt{\frac{4\pi}{2l+1}\Sigma_{m=-l}^{l}|\Sigma_f \frac{A(f)}{A}, Y_{lm}(\theta_f, \phi_f)|^2}. \tag{4}$$

Here $A(f)$ denotes the area of face f of the Voronoi cell around a reference particle, A is the total surface area of the Voronoi cell, θ_f and ϕ_f are the polar and azimuth angles of the outer normal vector connecting the reference particle to the vertex representing an adjacent particle. Neighbor lists are typically defined using a fixed cutoff radius around each particle, identifying nearby particles as neighbors. We use the Python package Freud to calculate the bond order parameters and use a Voronoi cell to determine the particle neighborhood rather than the standard distance criterion [28, 23]. The Voronoi-based method avoids the need for a predefined cutoff and yields more robust neighbor definitions, particularly in disordered systems. Bond orientational order parameters have been widely employed to study structural transitions in colloidal and ceramic systems, including crystallization, nucleation, and glass formation [39, 3]. Q_6 is most commonly used to identify crystal structures by matching the calculated values to

ICCS Camera Ready Version 2025
To cite this paper please use the final published version:
DOI: 10.1007/978-3-031-97564-6_19

reference values for specific crystal structures such as fcc or hcp. Therefore, we use Q_6 to characterize changes in local ordering of particles.

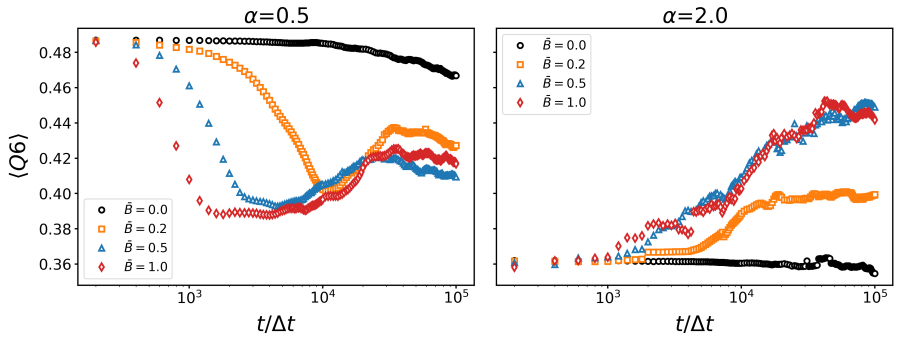

Fig. 6. Time evolution of the normalized six-fold Steinhardt bond orientational order parameter for bijels stabilized by oblate particles (left) and prolate particles (right), under varying magnetic field strengths.

For bijels stabilized by oblate particles a distinct decrease in $\langle Q_6 \rangle$ is observed upon application of a magnetic field, particularly at intermediate times. The drop becomes more pronounced with increasing field strength, suggesting that the field disrupts the initial local ordering as particles begin to tilt or reorient in response to magnetic torque. A partial recovery in ordering is seen at late times, likely due to re-jamming of particles into a new configuration. In contrast, bijels stabilized by prolate particles exhibit a monotonic increase in bond order with increasing $\bar{B}$, indicating that the applied field enhances local structural order rather than disrupting it. This is attributed to the alignment of prolate particles along the field direction, which promotes side to side packing and increases local orientational ordering. The absence of a dip in the ordering curve, even at intermediate times, further supports the idea that field-induced alignment in prolate systems occurs more smoothly and constructively compared to the more disruptive response in oblate-particle-stabilized bijels. These trends reflect the effect of particle shape on interfacial reorientation of particles and the effect of local particle packing.

The six-fold Steinhardt bond orientational order parameter $\langle Q_6 \rangle$ and the average interfacial angle $\langle \psi \rangle$ provide a detailed view of how external magnetic fields and particle shape influence the post-formation microstructural evolution of bijels. The parameter $\langle Q_6 \rangle$ quantifies the degree of local positional and orientational ordering among particles at the fluid interface. For oblate particles, a pronounced decrease in $\langle Q_6 \rangle$ under field application indicates a disruption of local packing, likely due to out-of-plane tilting that breaks the symmetry of the initially jammed monolayer. In contrast, for bijels stabilized by prolate particles, $\langle Q_6 \rangle$ increases steadily with field strength, suggesting that the applied field

ICCS Camera Ready Version 2025
To cite this paper please use the final published version:
DOI: 10.1007/978-3-031-97564-6_19

promotes enhanced order through cooperative alignment along the field direction. These contrasting trends emphasize the importance of particle anisotropy in determining how a magnetic field affects interfacial order.

The evolution of the average interfacial angle $\langle\psi\rangle$ further elucidates particle alignment dynamics under magnetic torque. For oblate particles, a continuous increase in $\langle\psi\rangle$ at late timesteps suggests gradual tilting out of the interface, which leads to vertical stacking and correlates with a reduction in local order. In contrast, prolate particles exhibit an initial increase in $\langle\psi\rangle$, followed by a plateau or decrease, indicating that after an initial tilt, particles tend to reorient to lie flatter on the interface, promoting side-to-side or end-to-end alignment and thus increasing $\langle Q_6\rangle$. Based on the results comparing the difference in microstructure between fields applied to bijels during and after formation show that the results are sensitive to the initial position of the particles. Further investigation is needed to determine whether microstructural variations are consistent and reproducible. Comparisons between bijels formed under a magnetic field and those exposed to a field post-formation show only minor differences in final microstructure, suggesting that the timing of field application may not be critical. Instead, the field-controlled orientation of particles appears to be the dominant factor governing the development of anisotropic domains, highlighting the potential of magnetic alignment as a post-processing tool for tuning bijel structure.

4 Conclusions

Motivated by the potential applications of bijels in catalyst supports, filtration membranes, and drug delivery systems, this study explores how bijels stabilized by magnetically responsive ellipsoidal particles can serve as a platform for designing active soft materials. Using hybrid Lattice Boltzmann–Molecular Dynamics simulations, we investigated the structural response of bijels stabilized by oblate and prolate particles, initially formed without a magnetic field and subsequently exposed to varying field strengths. Additionally, we compared these systems to bijels formed under identical magnetic field conditions to assess whether the timing of field application significantly influences the resulting microstructure.

Our results demonstrate how magnetic field application and particle shape jointly influence the microstructural evolution of bijels post-formation. Through the analysis of domain size, Steinhardt bond orientational order, interfacial angle, and 2D structure factors, we show that oblate and prolate particles respond in different ways to applied magnetic fields. Oblate particles tend to disrupt local order by tilting out of the interface under magnetic torque, resulting in reduced bond ordering and moderate anisotropic coarsening. In contrast, prolate particles promote field-aligned packing that enhances local ordering and also promoting moderate anisotropic coarsening.

The timing of field application, whether during or after bijel formation, was shown to influence the degree of anisotropy and ordering, though to a lesser extent than the shape-dependent particle response. Applying a magnetic field post-formation can induce similar structural features to those formed under field con-

ICCS Camera Ready Version 2025
To cite this paper please use the final published version:
DOI: 10.1007/978-3-031-97564-6_19

ditions, especially for prolate-stabilized systems, suggesting that post-processing with magnetic fields is a viable route for structural tuning. However, subtle differences observed in the structure factor distributions hint at sensitivity to initial particle arrangement, motivating further studies into the reproducibility and control of these transformations. Steric hindrance may decrease as particle size reduces, allowing particles to better conform to interface curvature, though the effects on the results with micron-sized particles remain unclear. The impact of changes in particle spacing on reactivity, selectivity, or diffusion rates is also not well understood. Furthermore, additional particle interactions, such as chemical crosslinking or charge, may influence these results, especially in applications requiring high shear resistance, such as cross-flow reactors and separation membranes. In conclusion, our simulations provide insights into the microstructure changes and mechanism underlying the stimuli response of bijels stabilized by ellipsoidal particles upon application of constant magnetic fields.

Acknowledgments. This work was supported by the National Science Foundation under NSF Award DMR-2414458 and OIA-2346036. Any opinions, findings and conclusions or recommendations expressed in this material are those of the authors and do not necessarily reflect those of the National Science Foundation. This work used NCSA Delta GPU at the National Center for Supercomputing Applications through allocation PHY220131 from the Advanced Cyberinfrastructure Coordination Ecosystem: Services & Support (ACCESS) program, which is supported by National Science Foundation grants #2138259, #2138286, #2138307, #2137603, and #2138296.

Disclosure of Interests. There are no conflicts to declare.

References

1. Aidun, C.K., Lu, Y., Ding, E.J.: Direct analysis of particulate suspensions with inertia using the discrete boltzmann equation. J. Fluid Mech. **373**, 287–311 (1998). https://doi.org/10.1017/S0022112098002493
2. Bago Rodriguez, A.M., Binks, B.P.: Capsules from pickering emulsion templates. Current Opinion in Colloid & Interface Science **44**, 107–129 (2019). https://doi.org/10.1016/j.cocis.2019.09.006
3. Besseling, R., Weeks, E.R., Schofield, A.B., Poon, W.C.K.: Three-Dimensional Imaging of Colloidal Glasses under Steady Shear. Physical Review Letters **99**(2), 028301 (2007). https://doi.org/10.1103/PhysRevLett.99.028301
4. Bhatnagar, P.L., Gross, E.P., Krook, M.: A model for collision processes in gases. i. small amplitude processes in charged and neutral one-component systems. Physical Review **94**(3), 511–525 (1954). https://doi.org/10.1103/PhysRev.94.511
5. Cha, S., Lim, H.G., Haase, M.F., Stebe, K.J., Jung, G.Y., Lee, D.: Bicontinuous interfacially jammed emulsion gels (bijels) as media for enabling enzymatic reactive separation of a highly water insoluble substrate. Sci Rep **9**(1), 6363 (2019). https://doi.org/10.1038/s41598-019-42769-8
6. Davies, G.B., Krüger, T., Coveney, P.V., Harting, J.: Detachment energies of spheroidal particles from fluid-fluid interfaces. J. Chem. Phys. **141**(15), 154902 (2014). https://doi.org/10.1063/1.4898071, publisher: American Institute of Physics

ICCS Camera Ready Version 2025
To cite this paper please use the final published version:
DOI: 10.1007/978-3-031-97564-6_19

7. Davies, G.B., Krüger, T., Coveney, P.V., Harting, J., Bresme, F.: Interface deformations affect the orientation transition of magnetic ellipsoidal particles adsorbed at fluid-fluid interfaces. Soft Matter **10**(35), 6742–6748 (2014). https://doi.org/10.1039/C4SM01124D
8. Ebner, M., Chung, D.W., García, R.E., Wood, V.: Tortuosity anisotropy in lithium-ion battery electrodes. Advanced Energy Materials **4**(5), 1301278 (2014). https://doi.org/10.1002/aenm.201301278
9. Fei, W., Gu, Y., Bishop, K.J.: Active colloidal particles at fluid-fluid interfaces. Current Opinion in Colloid & Interface Science **32**, 57–68 (2017). https://doi.org/10.1016/j.cocis.2017.10.001
10. Fei, W., Tzelios, P.M., Bishop, K.J.M.: Magneto-capillary particle dynamics at curved interfaces: Time-varying fields and drop mixing. Langmuir **36**(25), acs.langmuir.9b03119 (2020). https://doi.org/10.1021/acs.langmuir.9b03119
11. Garcia, A.E., Wang, C.S., Sanderson, R.N., McDevitt, K.M., Zhang, Y., Valdevit, L., Mumm, D.R., Mohraz, A., Ragan, R.: Scalable synthesis of gyroid-inspired free-standing three-dimensional graphene architectures. Nanoscale Adv. **1**(10), 3870–3882 (2019). https://doi.org/10.1039/C9NA00358D
12. Grattoni, C.A., Dawe, R.A., Seah, C.Y., Gray, J.D.: Lower critical solution coexistence curve and physical properties (density, viscosity, surface tension, and interfacial tension) of 2,6-lutidine + water. J. Chem. Eng. Data **38**(4), 516–519 (1993). https://doi.org/10.1021/je00012a008
13. Günther, F., Frijters, S., Harting, J.: Timescales of emulsion formation caused by anisotropic particles. Soft Matter **10**(27), 4977–4989 (2014). https://doi.org/10.1039/C3SM53186D
14. Herzig, E.M., White, K.A., Schofield, A.B., Poon, W.C.K., Clegg, P.S.: Bicontinuous emulsions stabilized solely by colloidal particles. Nature Mater **6**(12), 966–971 (2007). https://doi.org/10.1038/nmat2055
15. Hsieh, M.T., Begley, M.R., Valdevit, L.: Architected implant designs for long bones: Advantages of minimal surface-based topologies. Materials & Design **207**, 109838 (2021). https://doi.org/10.1016/j.matdes.2021.109838
16. Jansen, F., Harting, J.: From bijels to pickering emulsions: A lattice boltzmann study. Phys. Rev. E **83**(4), 046707 (2011). https://doi.org/10.1103/PhysRevE.83.046707, publisher: American Physical Society
17. Karthikeyan, N., Schiller, U.D.: Formation of bijels stabilized by magnetic ellipsoidal particles in external magnetic fields. Soft Matter **20**(45), 8952–8967 (2024). https://doi.org/10.1039/D4SM00751D
18. Kendon, V.M., Cates, M.E., Pagonabarraga, I., Desplat, J.C., Bladon, P.: Inertial effects in three-dimensional spinodal decomposition of a symmetric binary fluid mixture: a lattice boltzmann study. J. Fluid Mech. **440**, 147–203 (2001). https://doi.org/10.1017/S0022112001004682
19. Ladd, A.J.C.: Numerical simulations of particulate suspensions via a discretized boltzmann equation. part 1. theoretical foundation. J. Fluid Mech. **271**, 285–309 (1994). https://doi.org/10.1017/S0022112094001771
20. Lechner, W., Dellago, C.: Accurate determination of crystal structures based on averaged local bond order parameters. The Journal of Chemical Physics **129**(11), 114707 (2008). https://doi.org/10.1063/1.2977970
21. Lin, Q., Liu, K.H., Cui, Z.G., Pei, X.M., Jiang, J.Z., Song, B.L.: pH-responsive pickering foams stabilized by silica nanoparticles in combination with trace amount of dodecyl dimethyl carboxyl betaine. Colloids and

ICCS Camera Ready Version 2025
To cite this paper please use the final published version:
DOI: 10.1007/978-3-031-97564-6_19

Surfaces A: Physicochemical and Engineering Aspects **544**, 44–52 (2018). https://doi.org/10.1016/j.colsurfa.2018.02.027
22. Maingret, V., Courrégelongue, C., Schmitt, V., Héroguez, V.: Dextran-based nanoparticles to formulate pH-responsive pickering emulsions: A fully degradable vector at a day scale. Biomacromolecules **21**(12), 5358–5368 (2020). https://doi.org/10.1021/acs.biomac.0c01489
23. Mickel, W., Kapfer, S.C., Schröder-Turk, G.E., Mecke, K.: Shortcomings of the bond orientational order parameters for the analysis of disordered particulate matter. The Journal of Chemical Physics **138**(4), 044501 (Jan 2013). https://doi.org/10.1063/1.4774084
24. Misra, K.: Magnetic (electric) drop deformation in uniform external fields: Volume averaged methods and formation of static and dynamic conical tips. Physics of Fluids **32**(10), 107104 (2020). https://doi.org/10.1063/5.0023594
25. Nakayama, M., Kajiyama, S., Kumamoto, A., Nishimura, T., Ikuhara, Y., Yamato, M., Kato, T.: Stimuli-responsive hydroxyapatite liquid crystal with macroscopically controllable ordering and magneto-optical functions. Nat Commun **9**(1), 568 (2018). https://doi.org/10.1038/s41467-018-02932-7
26. Nourgaliev, R., Dinh, T., Theofanous, T., Joseph, D.: The lattice boltzmann equation method: theoretical interpretation, numerics and implications. International Journal of Multiphase Flow **29**(1), 117–169 (2003). https://doi.org/10.1016/S0301-9322(02)00108-8
27. Raju, R.R., Liebig, F., Klemke, B., Koetz, J.: pH-responsive magnetic pickering janus emulsions. Colloid Polym Sci **296**(6), 1039–1046 (2018). https://doi.org/10.1007/s00396-018-4321-z
28. Ramasubramani, V., Dice, B.D., Harper, E.S., Spellings, M.P., Anderson, J.A., Glotzer, S.C.: freud: A software suite for high throughput analysis of particle simulation data. Computer Physics Communications **254**, 107275 (Sep 2020). https://doi.org/10.1016/j.cpc.2020.107275
29. Rozynek, Z., Khobaib, K., Mikkelsen, A.: Opening and closing of particle shells on droplets via electric fields and its applications. ACS Appl. Mater. Interfaces **11**(25), 22840–22850 (2019). https://doi.org/10.1021/acsami.9b05194
30. Samdani, J.S., Kang, T.H., Zhang, C., Yu, J.S.: Bicontinuous spider network architecture of free-standing $MnCoO_X$ @NCNF anode for li-ion battery. ACS Omega **2**(11), 7672–7681 (2017). https://doi.org/10.1021/acsomega.7b01228
31. Santiago Cordoba, M.A., Spendelow, J.S., Parra-Vasquez, A.N.G., Kuettner, L.A., Welch, P.M., Hamilton, C.E., Oertel, J.A., Duque, J.G., Meierdierks, E.J., Semelsberger, T.A., Gordon, J.C., Lee, M.N.: Aerobijels: Ultralight carbon monoliths from cocontinuous emulsions. Adv Funct Materials **30**(6), 1908383 (2020). https://doi.org/10.1002/adfm.201908383
32. Shan, X., Chen, H.: Lattice boltzmann model for simulating flows with multiple phases and components. Phys. Rev. E **47**(3), 1815–1819 (1993). https://doi.org/10.1103/PhysRevE.47.1815
33. Shan, X., Chen, H.: Simulation of nonideal gases and liquid-gas phase transitions by the lattice boltzmann equation. Phys. Rev. E **49**(4), 2941–2948 (1994). https://doi.org/10.1103/PhysRevE.49.2941
34. Steinhardt, P.J., Nelson, D.R., Ronchetti, M.: Bond-orientational order in liquids and glasses. Physical Review B **28**(2), 784–805 (Jul 1983). https://doi.org/10.1103/PhysRevB.28.784
35. Stratford, K., Adhikari, R., Pagonabarraga, I., Desplat, J.C., Cates, M.E.: Colloidal jamming at interfaces: A route to fluid-bicontinuous gels. Science **309**(5744), 2198–2201 (2005). https://doi.org/10.1126/science.1116589

ICCS Camera Ready Version 2025
To cite this paper please use the final published version:
DOI: 10.1007/978-3-031-97564-6_19

36. Tang, J., Berry, R.M., Tam, K.C.: Stimuli-responsive cellulose nanocrystals for surfactant-free oil harvesting. Biomacromolecules **17**(5), 1748–1756 (2016). https://doi.org/10.1021/acs.biomac.6b00144
37. Tavacoli, J.W., Thijssen, J.H.J., Schofield, A.B., Clegg, P.S.: Novel, robust, and versatile bijels of nitromethane, ethanediol, and colloidal silica: Capsules, sub-ten-micrometer domains, and mechanical properties. Adv Funct Materials **21**(11), 2020–2027 (2011). https://doi.org/10.1002/adfm.201002562
38. Tham, F.K., Ng, W.M., Leong, S.S., Yeap, S.P., Low, S.C., Lee, H.L., Lim, J.: Magnetophoresis of magnetic pickering emulsions under low field gradient: Macroscopic and microscopic motion. Langmuir **37**(5), 1811–1822 (2021). https://doi.org/10.1021/acs.langmuir.0c03153
39. Vågberg, D., Olsson, P., Teitel, S.: Glassiness, rigidity, and jamming of frictionless soft core disks. Physical Review E **83**(3), 031307 (2011). https://doi.org/10.1103/PhysRevE.83.031307
40. Xie, Q., Davies, G.B., Harting, J.: Direct assembly of magnetic janus particles at a droplet interface. ACS Nano **11**(11), 11232–11239 (2017). https://doi.org/10.1021/acsnano.7b05550, publisher: American Chemical Society
41. Xie, Q., Harting, J.: Controllable capillary assembly of magnetic ellipsoidal janus particles into tunable rings, chains and hexagonal lattices. Adv. Mater. **33**(8), 2006390 (2021). https://doi.org/10.1002/adma.202006390
42. Yabuno, Y., Mihara, K., Miyagawa, N., Komatsu, K., Nakagawa, K., Shintani, T., Matsuyama, H., Yoshioka, T.: Preparation of polyamide-PVDF composite hollow fiber membranes with well-developed interconnected bicontinuous structure using high-temperature rapid NIPS for forward osmosis. Journal of Membrane Science **612**, 118468 (2020). https://doi.org/10.1016/j.memsci.2020.118468
43. Yang, H., Wang, S., Zhang, W., Wu, J., Yang, S., Yu, D., Wu, X., Sun, Y., Wang, J.: Rapid demulsification of pickering emulsions triggered by controllable magnetic field. Sci Rep **10**(1), 16565 (2020). https://doi.org/10.1038/s41598-020-73551-w
44. Zhang, L., Zhang, G., Ge, J., Jiang, P., Ding, L.: pH- and thermo-responsive pickering emulsion stabilized by silica nanoparticles and conventional nonionic copolymer surfactants. Journal of Colloid and Interface Science **616**, 129–140 (2022-06). https://doi.org/10.1016/j.jcis.2022.02.067
45. Zhang, X., Ju, Z., Housel, L.M., Wang, L., Zhu, Y., Singh, G., Sadique, N., Takeuchi, K.J., Takeuchi, E.S., Marschilok, A.C., Yu, G.: Promoting transport kinetics in li-ion battery with aligned porous electrode architectures. Nano Lett. **19**(11), 8255–8261 (2019). https://doi.org/10.1021/acs.nanolett.9b03824
46. Zhou, J., Qiao, X., Binks, B.P., Sun, K., Bai, M., Li, Y., Liu, Y.: Magnetic pickering emulsions stabilized by fe $_3$ o $_4$ nanoparticles. Langmuir **27**(7), 3308–3316 (2011). https://doi.org/10.1021/la1036844

ICCS Camera Ready Version 2025
To cite this paper please use the final published version:
DOI: 10.1007/978-3-031-97564-6_19